Blockage Robustness in Access Point Association for mmWave Wireless LANs with Mobility

Yuchen Liu and *Douglas M. Blough*
School of Electrical and Computer Engineering
Georgia Institute of Technology

2020 IEEE 45th Conference on Local Computer Networks (LCN) | 978-1-7281-7158-6/20/$31.00 ©2020 IEEE | DOI: 10.1109/LCN48667.2020.9314770

***Abstract*—Millimeter-wave wireless LANs are targeted for use with bandwidth-intensive applications such as virtual/augmented reality and real-time high-definition video. To maintain high throughput while addressing mmWave signal blockages, multiple access points (APs) within one room to improve line-of-sight conditions is considered a promising approach. In a scenario with fixed and mobile (human) obstacles, we mathematically analyze LoS blockages produced by mobility, and use the analysis to develop a multi-AP association scheme. Our scheme statically assigns primary and backup APs in order to maximize blockage robustness and perform load balancing among APs. Simulation results show that: 1) our static approach can provide blockage tolerance close to that of an expensive dynamic probing approach while achieving higher throughput, 2) the use of client mobility patterns, if known, can improve our static approach even further, and 3) our approach achieves significantly better fairness and load balancing than existing approaches.**

I. Introduction

Due to the current bandwidth shortage and ever-increasing demands of various bandwidth-hungry applications, millimeter-wave wireless local-area networks (mmWave WLANs) are receiving increased attention due to the availability of spectrum in the mmWave bands [1]. However, the narrow beamwidth antennas used in mmWave communications make the signals extremely sensitive to blockages as compared to their lower-frequency counterparts. Thus, line-of-sight (LoS) connectivity between access points (APs) and clients becomes critical to maintain link performance, since non-LoS (NLoS) paths suffer a large attenuation, which reduces their data rate substantially compared to LoS paths [2]–[4]. To overcome blockage effects caused by potential obstacles such as furniture, or even humans, in a typical indoor WLAN setting, a promising approach is to deploy multiple APs in the same room [5], as this offers more opportunities to establish LoS connections between clients and APs.

Some prior research [6] [7] studied multi-AP deployment issues in mmWave WLANs, e.g. in our previous work [7], placements of multiple APs that maximize LoS coverage in typical indoor scenarios were derived. Once an intelligent multi-AP placement is made, a good matching between APs and clients becomes critical for improving both network robustness and the users' quality of experience. To be practical, the AP association must account for mobility, both of the user devices as well as obstacles since even the human body is capable of obstructing mmWave signals.

In the IEEE 802.11ad standard [8], the AP association process is based on the highest received signal strength (RSS). However, in a typical indoor scenario with limited range, different mmWave APs that have LoS to a client actually provide very similar RSS and data transmission rates. Therefore, RSS might not be the best metric for an association policy. Instead, other metrics important for the network robustness and performance, such as the link reliability and AP load, should be taken into account.

In this work, we consider a ceiling-mounted multi-AP architecture in mmWave WLANs, such as was proposed in [7] [9]. In [7], it was shown how to optimally place APs on the ceiling, in order to maximize LoS coverage in the presence of fixed obstacles such as furniture, thereby increasing the likelihood that each client has an LoS path to at least one AP within a room. However, the mmWave LoS links are still susceptible to the mobility of clients and moving obstacles such as humans, which may disrupt the data transmissions or even make established connections fail. For this reason, we investigate a blockage-robust multi-AP association, which assigns primary and backup APs for each client based on quantified link reliability in the presence of mobility. The approach also can factor in the specific mobility patterns of clients if they are known. Different from prior works that have users associating with APs based on RSS or dynamically probed channel conditions, our work conducts a thorough analysis of complex environments, extracting the useful information about potential obstacles. Our analysis not only accounts for fixed obstacles but also accounts for temporary-blockage effects caused by moving obstacles and mobility of clients. The proposed multi-AP association scheme maximizes connection reliability for clients while also load balancing across APs.

Through extensive simulations, we evaluate the performance of several variations of our AP association scheme in different network scenarios. The results show that the network performance is superior to existing AP association approaches in multiple dimensions. In particular, our approaches have a blockage robustness comparable to the dynamic channel-probing approach, which checks for the best channel on each transmission, while our lower run-time overhead produces higher throughput. Furthermore, our approaches have better fairness and load balancing than existing approaches.

II. Related work

Several prior works have studied AP association problems in multi-AP mmWave WLANs [9]–[13]. In [10], the author formulated the AP matching problem as a partially observed

Markov decision process and obtained an optimal policy to maximize the network throughput. However, this work did not analyze potential blockages and only a single user was considered. In [9], two AP assignment schemes with different complexity were proposed and transmission time slot scheduling schemes were studied in a 60 GHz WLAN. In [11], a cluster-based user association scheme was presented, which was based on strongest received signal in mmWave femtocell networks and aimed to overcome the performance loss imposed by co-channel interference. In [12], the authors devised a multi-AP association framework based on multi-path TCP protocol and designed a flow-aware scheduling algorithm that optimizes transport layer performance. The authors of [13] studied the AP-client association problem to match each user having a rate requirement with an AP such that the maximum load among all APs is minimized, but potential blockage effects were not considered. These prior works mainly focused on maximizing network throughput or AP utilization without considering blockage robustness. Due to the blockage sensitivity of mmWave signals, the connection reliability of each AP-client pair is critical in avoiding outages and frequent AP switching, and a good AP association strategy should be capable of maintaining continuously high-rate transmissions for all connected AP-client pairs.

To avoid blockages as much as possible, some other works have users opportunistically select APs based on probing the channel conditions on every transmission [14]–[16]. As a typical example, [14] presented a mmWave opportunistic network model where users probe multiple APs in search of a channel that provides a maximum transmission rate. However, this dynamic probing approach incurs a high overhead, which can degrade data transmission efficiency and user throughput. Therefore, to avoid extra probing overhead and frequent AP switching, our work investigates an approach that combines a *statically computed* solution with low-complexity on-demand AP switching, where potential blockage effects caused by fixed obstacles, moving obstacles, and client mobility are quantified and pre-computed once for a given network environment. AP association decisions are made based on a novel robustness metric arising from our analysis, so as to achieve low-overhead and blockage-robust mmWave wireless communications.

III. System overview

In this section, we introduce the network architecture, AP deployment, and connectivity mode used in this paper.

A. Network model

We consider a centralized ceiling-mounted multi-AP network (CCMN) architecture for mmWave LANs, as shown in Fig. 1. In this architecture, multiple APs are mounted on the ceiling and serve the clients in the room, because this achieves better LoS coverage as compared to placing APs at a lower height, e.g. on the wall or on a desk or table [7]. We also assume that there is a centralized network controller in the back end, with all mmWave APs connected to this controller via wired connections. The controller is responsible for making association decisions based on inputs about active users in the network. Each AP collects information about the clients and sends it to the central controller, and then the controller conveys its decisions to the APs, which then notify the clients. With the wide deployment of high-speed Ethernet and optimized servers, such a centralized control architecture has been adopted for many different purposes in multi-AP WLANs in recent years [17], [18].

Although, traditionally, AP association decisions in WLANs have been left to the clients, we believe the substantial benefits of our centralized blockage-robust association mechanism, which are quantified in Section VI, are strong justification for adopting a centralized association scheme for mmWave multi-AP WLANs specifically.

In this work, we adopt a channel model accounting for both LoS and NLoS conditions in indoor mmWave communication, where the path loss model is extended to include multipath and shadowing components (more detail on the model is provided in Sec. VI-A). As is typical in mmWave network analysis, we adopt a narrow-beam directional antenna model for each wireless node, which means that antennas have a high gain within the main beam, and a much lower gain outside the main beam.

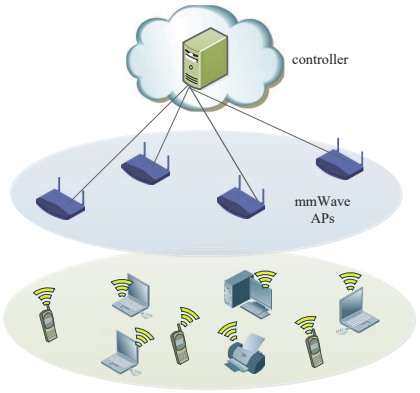

Fig. 1. The centralized ceiling-mounted multi-AP network architecture.

B. Infrastructure planning

It is known that the LoS connectivity is a critical requirement in mmWave WLANs, and the client can communicate with an AP at a high rate through the LoS path. In this work, we adopt the optimal placement of APs that was derived in our previous work [7]. With this intelligent approach, full LoS coverage of most indoor scenarios can be achieved with a few APs in the presence of fixed obstacles such as furniture. This ensures that each client can have at least one LoS AP, when considering the fixed obstacles.

C. Dual connectivity

Considering the fragile links in mmWave WLANs, today's IEEE 802.11ad standard incorporates a beam-searching mechanism that is triggered to find a new AP after the current path is blocked, but this is a time-consuming process that can take

up to a few seconds [19]. To tackle this problem, several works have proposed pre-establishing connections to several LoS APs with trained beams, associating to the primary AP that can potentially provide the best performance, and maintaining other paths in a backup mode for fast recovery [12], [20]–[25]. Since maintaining more than one backup link increases the beam-tracking overhead on clients, which could lower network performance [24], we consider the dual-connectivity mode [24], [25], i.e., each client will associate with one primary AP and one backup AP. With dual connectivity, an efficient beam tracking mechanism, such as in [26]–[28], can be used for fast AP switching once the blockage occurs. In this way, the link connectivity can be efficiently maintained with a small overhead.

IV. Quantification of Blockage Tolerance in Multi-AP mmWave WLANs

In this section, we give a mathematical framework to analyze the reliability of mmWave links, and quantify the blockage effects caused by moving obstacles and mobility of clients, which are referred to as the moving-obstacle tolerance (MOT) and the client-mobility tolerance (CMT), respectively.

A. Moving-obstacle tolerance

In this part, we first consider temporary-blockage effects caused by humans or movable objects in a typical indoor scenario, which may block established LoS connections between APs and clients. The problem we consider in this section is as follows. Assuming a mmWave WLAN with full LoS coverage and based on the dual-connectivity mode, find a pair of APs with maximum MOT from all of client's LoS APs.

Here, we use geometric analysis to quantify MOT of two LoS links of a client, and the derived result, as we show later, can also be applied for the case when there exists a single LoS link or no LoS links for some client. Based on the random shape theory from [30], obstacles such as temporarily stopped humans are assumed to form a Boolean scheme of rectangles, in which the centers of the rectangles fall within the room and form a homogeneous Poisson point process (PPP) C of density λ, where λ is the mean number of obstacles in an unit area. The width, W, and length, L, are assumed to be i.i.d. distributed and follow normal distributions, i.e. $W \sim \mathcal{N}(\mu_w$ ${\sigma_w}^2)$ and $L \sim \mathcal{N}(\mu_l, {\sigma_l}^2)$. The orientation distribution Θ of every obstacle is uniform over $[0, \pi]$. In this way, a random obstacle is characterized by the quadruple $\{c, w, l, \theta\}$, which is generated by sampling the distributions C, W, L, Θ.

From the 2-dimensional perspective in Fig. 2, when the client has two LoS connections with its primary and backup APs (eg. AP_1 and AP_2), the blockage region (e.g., S_1, S_2, and $S_{1,2}$) is determined by the size of the obstacle, the separation distances between the client and its LoS APs, and the intersected angle of two LoS links. For example, if the center of an obstacle falls in the blockage region S_1, only the link between client and AP_1 will be blocked, but if the center of obstacle falls in the blockage region $S_{1,2}$, both of the LoS links will be blocked. In what follows, we derive the probability that at least one of the LoS links is still connected in the presence of multiple obstacles, which we use as the metric of MOT.

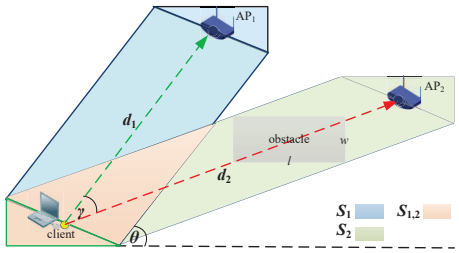

Fig. 2. Blockage area of two LoS links.

First, we derive the blockage area A_i (i.e. the area of $S_i \cup S_{1,2}$, $i \in [1, 2]$) in Eq. (1), and one LoS link between client and AP_i is blocked if the center of an obstacle falls in the blockage region $S_i \cup S_{1,2}$.

$$\begin{cases} A_1 = d_1 \cdot (|\cos\theta| \cdot w + |\sin\theta| \cdot l) + w \cdot l \\ A_2 = d_2 \cdot [|\cos(\theta-\gamma)| \cdot w + |\sin(\theta-\gamma)| \cdot l] + w \cdot l, \end{cases} \tag{1}$$

where d_i is the horizontal distance between AP_i and client, w, l, θ are the obstacle's width, length and orientation, respectively. Then, let random variable K denote the total number of random obstacles blocking the link between client and AP_i, and its expectation is derived as:

$$\begin{aligned} E[K]_{A_i} &= \int_W \int_L \int_\Theta \frac{1}{\pi} A_i(w,l,\theta,d) f_W(w) f_L(l)\ dw\ dl\ d\theta \\ &= \frac{2d_i \cdot (\mu_w + \mu_l)}{\pi} + \mu_w \cdot \mu_l. \end{aligned} \tag{2}$$

Second, both two LoS links will be blocked if the center of obstacle B falls in the overlapped blockage region S_{ol} (i.e., $S_{1,2}$), and this overlapping blockage area can be derived through geometric analysis as follow:

$$\begin{cases} (\frac{1}{2}\cot\gamma \cdot \cos^2\theta + \frac{1}{4}\sin 2\theta)w^2 - l^2 \cdot (\frac{1}{4}\sin 2\theta - \frac{1}{2}\cot\gamma \cdot \\ \sin^2\theta) + (\frac{1}{2}\cot\gamma \cdot \sin 2\theta - \frac{1}{2}\cos 2\theta + \frac{1}{2}) \cdot lw, & \gamma < \theta \le \pi \\ \frac{\cos\theta \cdot \cos(\theta-\gamma)}{2\sin\gamma} \cdot w^2 + l \cdot w, & \alpha < \theta \le \gamma \\ l \cdot w, & 0 < \theta \le \alpha, \end{cases} \tag{3}$$

where α equals to $\max\{0, \gamma - \pi/2\}$, and γ is the intersected angle of two LoS links. Then we further compute the expectation of K blocking both two LoS links as:

$$\begin{aligned} E[K]_{ol} &= \frac{1}{\pi} \int_W \int_L \int_\Theta S_{ol}(w,l,\theta) f_W(w) f_L(l)\ dw\ dl\ d\theta \\ &= \frac{({\mu_w}^2 + {\sigma_w}^2)}{\pi}[\frac{1}{4}(\pi-\alpha)\cot\gamma - \frac{\sin(2\alpha-\gamma)}{8\sin\gamma} - \frac{1}{4}\cos^2\gamma + \frac{1}{8}] \\ &\quad + \frac{({\mu_l}^2 + {\sigma_l}^2)}{\pi}[\frac{1}{4}(\pi-\gamma)\cot\gamma + \frac{1}{4}\cos^2\gamma] + \frac{\mu_w \cdot \mu_l(\pi+\gamma)}{2\pi}. \end{aligned} \tag{4}$$

In the following parts, we use E_{A_i} and E_{ol} in place of $E[K]_{A_i}$ and $E[K]_{ol}$ for simplicity.

Now we introduce the height effects of obstacles and extend the blockage model to 3 dimensions. It is known that an obstacle[1] intersecting the link between client and AP with a horizontal length of d blocks the LoS path if and only if its height $h_o > h_x$, where $h_x = H_A + \frac{x}{d} \cdot (h_c - H_A)$, and H_A and h_c are the height of AP and client ($H_A > h_c$), respectively.

Since the heights of obstacles are usually different in reality, we assume that the obstacle's height h_o follows the uniform distribution $H \sim U(a_o, b_o)$. Thus, in this 3-dimensional model, each obstacle $B(w, l, h, \theta)$ is extended to be characterized by the quintuple $\{c, w, l, h, \theta\}$. Given an obstacle intersects the LoS path between AP and client from 2D view, the conditional probability that an obstacle blocks the LoS path from 3D perspective is:

$$\begin{aligned} \varepsilon &= \tfrac{1}{d} \textstyle\int_0^d P[h > h_x] \, d_x \\ &= 1 - \int_0^1 \int_0^{y \cdot H_c + (1-y) H_A} f_H(h) \, dh \, dy \\ &= 1 - \tfrac{1}{b_o - a_o} \int_0^1 [\max\{\min\{b_o, v\}, a_o\} - a_o] \, dy \\ &= \tfrac{b_o + a_o - 2h_c}{2(H_A - h_c)}, \end{aligned} \tag{5}$$

where $v = yH_c + (1-y)H_A$. According to the PPP thinning property, the expectation $E[K]'$ in 3D blockage model is $\varepsilon E[K]$ for incorporating the height effect of obstacles [31]. As such, based on Eq. (2)-(5), we arrive at the probability that at least one of the LoS links is connected with multiple random obstacles as:

$$\begin{aligned} P_{MOT} = P(A_1 \cup A_2) &\overset{(a)}{=} \Pr(A_1) + \Pr(A_2) - \Pr(A_1 \cap A_2) \\ &\overset{(b)}{=} \sum_i \exp(-\lambda \cdot \varepsilon E_{A_i}) - \exp[-\lambda \cdot \varepsilon (\sum_i E_{A_i} - E_{ol})], \end{aligned} \tag{6}$$

where (a) is true because of the inclusion-exclusion principle, and (b) follows the basic property of homogeneous Poisson distribution with density λ. Taking Eq. (2)-(5) into Eq. (6), we obtain the close-form expression of probability that at least one of the LoS links is survival, which indicates the MOT of a client with a pair of APs. Note that P_{MOT} is equal to $Pr(A_i) = \exp(-\lambda \cdot \varepsilon E_{A_i})$ $(i = 1, 2)$ if there exists only one LoS AP$_i$, and P_{MOT} drops to zero when no LoS APs exist.

Given some specific parameters about obstacles[2], we investigate how the horizontal distance d_i and intersected angle of two LoS links γ affect the moving-obstacle tolerance. In Fig. 3, it is observed that the moving-obstacle tolerance decreases as d_i increases since it has more potential to experience blockages between APs and a client[3]. On the other hand, as γ increases, the moving-obstacle tolerance is improved, and this is because the overlapping blockage area of two LoS links will decrease, which is likely to reduce the likelihood of blocking both LoS links simultaneously with a single obstacle.

[1]Here the object with the height larger than general height of client is considered as the obstacle, since objects with very small heights will have no effect on LoS paths between ceiling-mounted APs and clients.

[2]Here we set $\mu_l = 0.5$, $\sigma_l = 0.1$, $\mu_w = 0.25$, $\sigma_w = 0.05$, $a_o = 0.5$, $b_o = 1.9$, $h_c = 0.6$ and $H_A = 3$.

[3]In Fig. 3, we assume $d_1 = d_2$ for simplicity since they have the equivalent effects on MOT according to Eq. (6).

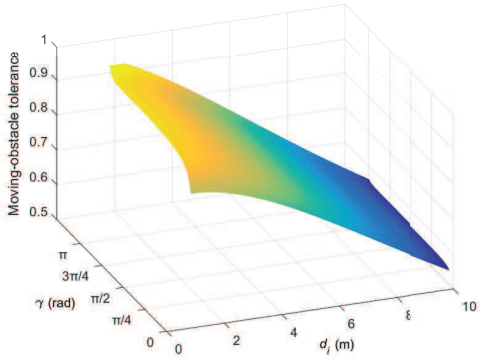

Fig. 3. P_{MOT} vs. d_i and γ.

B. Client-mobility tolerance

Considering the mobility characteristics of clients in a typical indoor scenario based on [32], the client has potential to move around or temporarily stay at some places other than its home location. During the period of leaving its home location, the primary LoS link and even backup link might be blocked by existing fixed obstacles or moving obstacles, therefore, we quantify the client-mobility tolerance (CMT) of each pair of LoS APs, accounting for both fixed- and moving-obstacle effects. Note that the derived results in this section can also be applied for the single LoS-AP case or no LoS-AP case for some client.

Here we discuss the approaches to quantify CMT with/without knowledge of mobility patterns of clients as follows.

1) Without mobility patterns: Based on our previous work [7], [33], the *grid-based search (GSS) algorithm* was proposed to efficiently find the shadowing regions (SR) caused by fixed obstacles in terms of different APs, where the rectangular room is divided into a large number of small grids with side length l_g (e.g., see Fig. 4), and we can find all shadowed grids (SG) whose center points fall in SRs. The grids outside those SRs are referred to as the non-shadowed grids (NG), and the LoS connection can be maintained if the client moves to these NGs rather than SGs in the presence of fixed obstacles.

For a given shadowing-region map, we can incorporate the moving-obstacle effects at each NG, and derive the probability that the LoS link is still connected when the client leaves its home location and moves around within the room, which accounts for both fixed and moving obstacles as follows:

$$\begin{aligned} P_{CMT} &\overset{(c)}{=} \sum_{i \in NG} \Pr(i \in NG) \cdot \Pr(\text{LoS} | i \in NG) \\ &= \sum_{i \in NG} \frac{1}{n_g} \cdot P_{MOT_i} = \frac{{l_g}^2}{r_l \cdot r_w} \cdot \sum_{i \in NG} P_{MOT_i}, \end{aligned} \tag{7}$$

where (c) is based on the total probability theorem, n_g is the total number of grids, r_l and r_w are the room's length and width, respectively, and P_{MOT_i} is the MOT at the non-shadowed grid i, which can be computed by Eq. (6). Here P_{CMT} is considered as the key performance index of CMT. Of particular note, Eq. (7) can quantify CMT for any cases no matter how many LoS APs of a client existing in the scenario, especially P_{CMT} drops to zero when no LoS AP exists for some client since there are no NGs in the shadowing-region map.

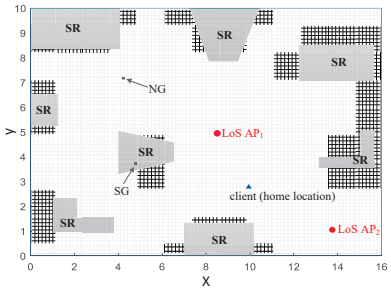

Fig. 4. The shadowing-region map for a client and its associated APs.

2) With mobility patterns: Here we discuss the approach to quantify CMT if the mobility patterns of clients are known.

During a period of time, we can investigate the client mobility features by recording their frequently visited locations (FL) within the room. When the client leaves its home location and moves around, it tends to visit those hotspot locations (i.e., FLs) and temporarily stays for some time [32]. By collecting this mobility information, we can obtain a mobility-pattern map for each client (e.g., as shown in Fig. 5), in which the popularity weight P_w of each FL (shown with the stars) indicates the time percentage taken by the client at this FL.

With the knowledge of FLs, we only need to consider whether or not the candidate APs can cover those FLs. We can, therefore, extend Eq. (7) to derive the CMT in terms of the popularity weights P_w of the known FLs as follows:

$$\begin{aligned} P_{CMT} &= \sum_{i \in NG} \frac{1}{n_g} \cdot \mathbb{I}_{FL}(i) \cdot P_{MOT_i} \cdot P_{w_i} \\ &= \frac{{l_g}^2}{r_l \cdot r_w} \cdot \sum_{i \in NG} \mathbb{I}_{FL}(i) \cdot P_{MOT_i} \cdot P_{w_i}, \end{aligned} \tag{8}$$

where $\mathbb{I}_{FL}(\cdot)$ is the indicator function, which is equal to 1 if NG_i covers one of FLs, otherwise it is 0. The popularity weight P_{w_i} of NG_i is equal to the P_w of its covered FL. Note that the blockage tolerance on pathways between visited locations is ignored here since the walking time is quite short as compared to the pause time at each FL in a typical indoor scenario, and the walking time therefore has a negligible impact on network performance[4].

C. Robustness index

Based on preceding analyses, considering both moving-obstacle and client-mobility effects, we finally define a robustness index (RI) that takes both MOT and CMT into account as follow:

[4]The detailed validation results are omitted here due to the space limitation, but they show that factoring in blockages on clients' pathways only causes less than a 1% performance drop with typical pause times at FLs.

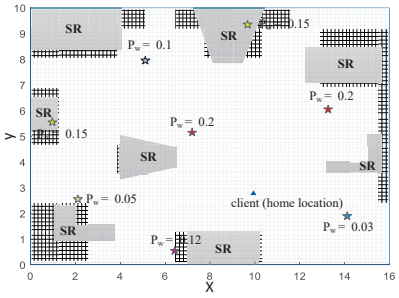

Fig. 5. The mobility-pattern map for a client.

$$\text{RI} = (1-\eta) \cdot P_{MOT_h} + \eta \cdot P_{CMT}, \tag{9}$$

where P_{MOT_h} denotes the MOT at the home location of client, and $\eta \in [0, 1)$ is a client-mobility factor that indicates how frequently the client leaves its home location and moves around. For instance, the smaller η (<0.5) should be chosen if the client spends over 50% of time staying at its home location, otherwise we set η to a larger value (>0.5) if the client has more tendency to move around. This derived metric will be utilized in our association protocol design in the next section.

V. Blockage-robust multi-AP association scheme

In this section, we present a multi-AP association approach, which adopts either a highly reliable multi-AP selection algorithm, referred to as HRS, or a modified version, referred to as AHRS, which achieves better load balancing across APs.

A. Highly reliable multi-AP selection algorithm

In multi-AP mmWave WLANs, consistently high user throughput is mainly dependent on two factors: 1) the reliability of connections, and 2) the load on the APs. An AP may become overloaded if a large number of clients are associated with it, which would significantly degrade the users' quality of experience since fewer resources can be allocated for each client on the overloaded AP. In this part, we propose a highly reliable multi-AP selection (HRS) algorithmm, which considers both connection reliability and AP load.

Algorithm 1 shows the pseudocode of Algorithm HRS. In the input, S_{ap} and U are sets that contain location information of placed APs and clients within the room, respectively, and Obs includes the dimensions and positions of fixed obstacles. D is a set that contains the data demands of clients. First, the LoS status between each placed AP and client u_k is checked, and then we include all LoS APs of u_k in LS_k (Lines 1-6). Next, the robustness index $RI_{i,j}$ for each pair of LoS APs is calculated based on the analytical model in Sec. III-C, and we choose the AP pair with maximum RI as candidate for u_k (Lines 11-14). In this way, the AP pairs that establish the most reliable connections for corresponding clients are obtained, and then we start to do the load balancing procedure among all selected APs of clients. It is known that LoS is

critical to provide high throughput in mmWave networks [2], and the performance benefits brought by different LoS APs becomes very close due to the limited range of a typical indoor scenario. Therefore, we allow either AP from the selected AP-pair for a given client to be chosen as its primary AP. Then, for load balancing purposes, we can formulate the primary-AP selection problem so as to minimize the maximum AP load as follows:

$$\min \quad L_{\max} \tag{10}$$

$$s.t. \quad L_{\max} \geq \frac{1}{R_i} \cdot \sum_{k \in U} D_k \cdot x_{k,i}, \quad \forall i \in S_{ap} \tag{11}$$

$$\sum_{i \in pr_k} x_{k,i} = 1, \quad \forall k \in U \tag{12}$$

$$x_{k,i} = 0, \ \forall i \notin pr_k, \ \forall k \in U, \tag{13}$$

where the continuous variable L_{max} is the *maximum load* over all APs, which is a metric for WLAN network performance that explains qualitatively congestion of network service [34], R_i is the maximum data rate provided by mmWave AP$_i$, D_k indicates the data demand of each client, and $x_{k,i}$ is the association indicator, which is set as 1 if AP$_i$ is assigned as the primary AP to client k, and otherwise it is 0. The objective in Eq. (10) combined with the constraint in Eq. (11) is to minimize the maximum traffic load utilization of each AP. Eq. (12) and Eq. (13) are shown as the primary-AP assignment constraints, which indicate that only one primary AP should be assigned for each client, and the APs not in the selected AP-pair of client k cannot be assigned as the primary AP. The problem formulated above is a mixed integer-linear programming problem, which can be solved by optimization software such as CPLEX [35].

Algorithm 1 Highly Robust Multi-AP Selection (HRS)

Input: S_{ap}, U, Obs, D
Output: mAP, bAP
1: **for** each client u_k in U **do**
2: **for** each AP_i in S_{ap} **do**
3: **if** CheckLoS(u_k, AP_i, Obs) = $true$ **then**
4: LS_k.add = AP_i; // LoS-AP set
5: **end if**
6: **end for**
7: **if** size(LS_k) = 1 **then**
8: $pair(u_k)$ = $LS_k(1)$; // for single-LoS AP case
9: **continue**;
10: **end if**
11: **for** each pair of AP $p_{i,j}$ in LS_k **do**
12: $\mathrm{RI}_{i,j} = (1-\eta) \cdot P_{MOT_h} + \eta \cdot P_{CMT}$;
13: **end for**
14: $pair(u_k)$ = $\arg\max\{RI_{i,j}\}$;
15: **end for**
16: AP^*_{id} = SolveOpt($pair$, U); // Eq. (10)-(13)
17: **for** each client u_k in U **do**
18: $mAP.u_k$ = $AP^*_{id}(u_k)$; // assign primary AP
19: $pair_{u_k}$.rmv($mAP.u_k$); // update $pair$ set
20: $bAP.u_k$ = $pair_{u_k}$(remaining AP); // add backup AP
21: **end for**
22: **return** mAP, bAP;

Back to Algorithm 1, after obtaining the optimal solution of this load-balancing process (Line 16), the primary AP and backup AP for each client will be assigned (Lines 17-21). Note that if only one LoS AP exists for a client, it will be directly selected as primary AP, and no backup AP will be assigned (Lines 7-10).

Based on the HRS algorithm and the knowledge of client-mobility information, we derive two multi-AP association schemes: 1) the *mRI* scheme, which uses Eq. (7) to calculate the robustness index (see Eq. (9)) and is applied to the scenario where the mobility patterns of clients are unknown; and 2) the *mRI-MP* scheme, which uses Eq. (8) to calculate the robustness index and is used for the scenario where the mobility patterns of clients are known.

B. Alternative approach to improve load balancing

In some network scenarios where the mobility patterns of clients are unknown, the load balancing across APs might be unsatisfactory after running HRS algorithm (as we show later in Sec. V-D), because most of the clients were originally assigned the same APs to maximize blockage tolerance. To avoid this situation, we propose an alternative AP selection approach (AHRS) that can be used if load balancing across APs is of equal importance with blockage tolerance. The AHRS scheme assigns APs for each client by jointly optimizing AP load and link reliability. In this way, it may worsen the connection robustness of a few clients, but can achieve better load balancing than the result produced by the HRS algorithm.

Here we introduce the AHRS approach in detail. Considering the robustness index of different AP pairs, if a primary AP (mAP$_i$) of one client is selected, the corresponding optimal backup AP (bAP$_i$) with the maximum RI among all LoS APs will be determined, i.e.,

$$\mathrm{bAP}_i = \underset{j \in LS, j \neq i}{\arg\max} RI_{i,j}, \tag{14}$$

In what follows, we solely focus on the primary-AP selection of each client, since once the mAP is assigned, the corresponding backup AP can be matched by solving Eq. (14).

Based on the above discussion, the optimization problem of jointly maximizing the link reliability and load balancing among APs can be described by Eq. (15)-(20):

$$\max \quad r_{\min} \tag{15}$$

$$s.t. \ \ r_{\min} \leq \frac{RI_k}{L_k}, \quad \forall k \in U \tag{16}$$

$$RI_k = \sum_{i \in LS_k} \max_{j \neq i, j \in LS_k} \{RI^k_{i,j}\} \cdot x_{k,i}, \quad \forall k \in U \tag{17}$$

$$L_k = \sum_{i \in LS_k} (x_{k,i} \cdot \frac{1}{R_i} \cdot \sum_{k \in U} D_k \cdot x_{k,i}), \ \ \forall k \in U \tag{18}$$

$$\sum_{i \in LS_k} x_{k,i} = 1, \quad \forall k \in U \tag{19}$$

$$x_{k,i} = 0, \ \forall i \notin LS_k, \ \forall k \in U, \tag{20}$$

where r_{min} is an auxiliary continuous variable, RI_k is the continuous variable, which indicates the robustness index of client k determined by assigned primary AP$_i$, L_k is the load utilization of assigned AP of client k, R_i and D_k are the maximum data rate of AP$_i$ and data demand of client k, respectively, and $x_{k,i}$ is the binary variable indicating if AP$_i$ is assigned as the primary AP to client k. The objective in Eq. (15) combined with the constraint in Eq. (16) is to maximize the minimum of ratio of RI_k and L_k, which aims to jointly optimize the robustness index of a client and the load utilization of a AP. Eq. (17) and Eq. (18) show the methods to obtain RI_k and L_k. Eq. (19) and Eq. (20) are the primary-AP assignment constraints.

We note that the above problem is a Mixed-Integer Non-Linear Problem (MINLP). Although MINLP is NP-hard, we solve it in our later simulations with the Bonmin toolbox [36], which is based on a branch-and-bound method [37] and produces a solution, but the relatively long running time makes this approach (referred to as $\mathrm{AHRS_{opt}}$) impractical for network configuration, especially when the scale of network becomes larger. Therefore, in what follows, we introduce a heuristic approach for AHRS to efficiently provide multi-AP association load-balanced solutions.

Algorithm 2 A-mRI: Alternative highly robust multi-AP selection

Input: S_{ap}, U, Obs, D
Output: mAP, bAP
1: LS = getLoSAP(U, S_{ap}, Obs);
2: RI = getRI(U, LS);
3: L_i = 0 ($i \in S_{ap}$); // init the load of each AP
4: **while** $size(U) \neq 0$ **do**
5: U_{id} = $\arg\min_{k \in U}\{size(LS_k)\}$;
6: **if** $size(U_{id}) > 1$ **then**
7: **for** each client u_k in U_{id} **do**
8: **for** each AP_i in LS_k of u_k **do**
9: $rt_i = (\max_{j \in LS_k, j \neq i} RI_{i,j})/(D_k + L_i)$;
10: **end for**
11: $u_m = \arg\max\{rt_i\}$;
12: **end for**
13: **end if**
14: **for** each AP_j in LS_m of u_m **do**
15: $rt_j = (\max_{i \in LS_m, i \neq j} RI_{j,i})/(D_m + L_j)$;
16: **end for**
17: $mAP_i = \arg\max\{rt_j\}$; // primary AP for u_m
18: $bAP_i = \arg\max_{j \in LS_m, j \neq i} RI_{i,j}$; // backup AP for u_m
19: $L_i = L_i + D_m$; // update the load of mAP_i
20: U.rmv(u_m);
21: **end while**
22: **return** mAP, bAP;

The pseudocode for our heuristic solution, referred to as A-mRI, is shown in Algorithm 2. We first obtain LoS APs and robustness indexes of different LoS link pairs for each client (Lines 1-2), which is the same procedure as in Algorithm 1 (see Lines 1-13). Then, the client having the minimum number of LoS APs will be first assigned APs (Line 5). Note that if there exist multiple clients having the same number of LoS APs in U_{id}, we start with the client u_m who has the maximum ratio of robustness index and AP load rt among all its LoS APs (Lines 6-11). After that, the AP with maximum rt is chosen as the primary AP for the client u_m (Lines 14-17), and the corresponding optimal backup AP is determined (Line 18). Finally, the data demand of client u_m should be added on the load of its selected primary AP (Line 19), and the algorithm is terminated once all clients have been matched with their APs (Line 4, 21).

C. Reconfiguration with network changes

In WLANs, the network state is changed whenever a new client arrives or an existing client departs. Recomputing all AP assignments every time the network state changes might incur a large overhead and unnecessarily disrupt current associations. Therefore, we adopt a threshold-based strategy to periodically reconfigure the network only after the network state has changed substantially.

As shown in Algorithm 3, when a new client u joins the network, if the number of state changes since the previous full reconfiguration divided by the total number of clients in the network exceeds a threshold value ϵ, we re-run the HRS or AHRS algorithm to reconfigure the entire network (Lines 5-8). Otherwise, we only conduct the AP assignment for that new client (Lines 9-10). In a similar way, when an existing client leaves the network, the reconfiguration process is triggered only if the percentage of changed clients since the last full reconfiguration exceeds ϵ (Lines 16-19).

Algorithm 3 Threshold-based reconfiguration

Input: S_{ap}, u, Obs, D, N_{orig}, N_{cur}, N_{change} ϵ
Output: mAP, bAP
1: **if** the arrival of u **then**
2: $N_{change} = N_{change} + 1$;
3: N_{cur} = N_{cur} + 1;
4: **do** Alg. 1 (Lines 2-14); // do calculations for u
5: **if** $N_{change}/N_{orig} \geq \epsilon$ **then**
6: **do** Alg. 1 (lines 16-21) or Alg. 2 (lines 3-21);
7: $N_{orig} = N_{cur}$; // reset the number of clients
8: $N_{change} \leftarrow 0$;
9: **else**
10: AssignAP(u, $pair$); // directly assign APs
11: **end if**
12: **end if**
13: **if** the departure of u **then**
14: $N_{change} = N_{change} + 1$;
15: $N_{cur} = N_{cur} - 1$;
16: **if** $N_{change}/N_{orig} \geq \epsilon$ & $N_{cur} > 1$ **then**
17: **do** Alg. 1 (lines 16-21) or Alg. 2 (lines 3-21);
18: $N_{orig} = N_{cur}$; // reset the number of clients
19: $N_{change} \leftarrow 0$;
20: **end if**
21: **end if**
22: **return** mAP, bAP;

VI. Simulation Results

In this section, we evaluate the network performance of our mRI, mRI-MP, and A-mRI algorithms in multi-AP mmWave LANs. In addition, we also choose some common AP association schemes as comparison points: 1) the strongest RSS AP

connection scheme (*StrongCon*), where each client associates to the AP with the strongest received signal strength and maintains that association as it moves around the room, which is the mechanism specified in the IEEE 802.11ad standard; 2) the dynamic channel probing scheme (*ProbeCon*) from [14], where the client searches for the AP with the best channel condition before every transmission, which has a high probing overhead and frequent AP switching but provides good blockage tolerance; and 3) a naive random AP pair association scheme (*RandCon*), i.e., first randomly choosing a pair of LoS APs for each client, and then randomly assigning the primary and backup APs from the chosen pair.

A. Simulation settings

1) Network scenario: We consider a typical indoor scenario in a lab room (16m×10m×3m), with a number of fixed obstacles (e.g., furniture) that are modeled as cuboids and placed on the floor. The center of each fixed obstacle follows a Poisson point process with a specific density ($\lambda = 0.1$), the width, length, and height follow truncated normal distributions (W$\sim$ $\mathcal{TN}$(0.56, 0.08, 0.25, 1.25), L$\sim$ $\mathcal{TN}$(1.08, 0.18, 0.5, 1.75) and H$\sim$ $\mathcal{TN}$(1.2, 0.6, 0.5, 1.9)), and the orientation follows a uniform distribution $\Theta \sim \mathcal{U}(0, \pi)$. Fig. 6 (a) shows a scenario example with a number of generated fixed obstacles. Then, by running the optimal multi-AP placement algorithm in [7], we deploy the APs in specific positions such that the network achieves full-coverage operation, e.g., the five APs shown in Fig. 6 (a), and each randomly-located client can find at least one LoS APs for high-rate communication. Here each wireless device is viewed as a random and uniformly distributed point in the 2-D area of a room and its height follows the uniform distribution $\mathcal{U}(0.3, 1.5)$. Besides the initial generated clients, the arrival of new clients and the departure of existing clients follow a Poisson distribution, where the expected time interval is set as 1 minute since each of our simulation case will last about 20 minutes, and the threshold ϵ for network reconfiguration is set to 0.2, i.e. a new global AP assignment is computed only when 20% of the clients have changed since the last global assignment. The distribution parameters for obstacles and clients were chosen by using a real-life lab environment as a guiding example. All length units are in meters throughout the paper.

2) Mobility model: To model the mobility characteristics of clients, who also act as moving obstacles, we adopt the mobility modeling approach from [38], [39] (referred to as Kim Kotz Kim model in Chapter 10.2 of [38]), which was shown to generate realistic movement traces in WLANs since the synthetic tracks highly match real tracks with a small relative error. First, we generate 15 hotspot locations with different popularity weights. For each moving obstacle or client, the next destination point is determined by the popularity weights of those hotspot locations, and the mobile entity moves on a straight-line path from the current location to the next one. Both the pause time at each destination point and the speed of movement follow the log-normal distribution, where the speed $ln(v)\sim\mathcal{N}$(-0.05, 0.69) (the mean is 1.21m/s) and pause time $ln(t_p)\sim\mathcal{N}$(3.15, 0.70) (the mean is 30.0s).

3) Obstacle model: The moving obstacles are modeled as cuboids, where their lengths, widths and heights follow truncated normal distributions (L$\sim$ $\mathcal{TN}$(0.5, 0.1, 0.2, 0.9), W$\sim$ $\mathcal{TN}$(0.25, 0.05, 0.1, 0.5), and H$\sim$ $\mathcal{TN}$(1.68, 0.25, 1.4, 1.9)). Obstacle orientations follow the uniform distribution $\Theta \sim \mathcal{U}(0, \pi)$.

Fig. 6 (b)-(d) show some sample cases, where a number of clients are distributed at their respective home locations within the room (shown with blue triangles). By adopting mRI, mRI-MP, and A-mRI schemes, we get the multi-AP association result for each client in Fig. 6 (b), (c) and (d), respectively, where each client connects to its assigned primary AP (shown with red dashed line), and the assigned AP pair including the backup AP is shown with the annotated numbers around the client. Depending on different multi-AP selection algorithms, and whether or not the mobility patterns are known, it is observed that clients will be associated with different APs in the same network scenario.

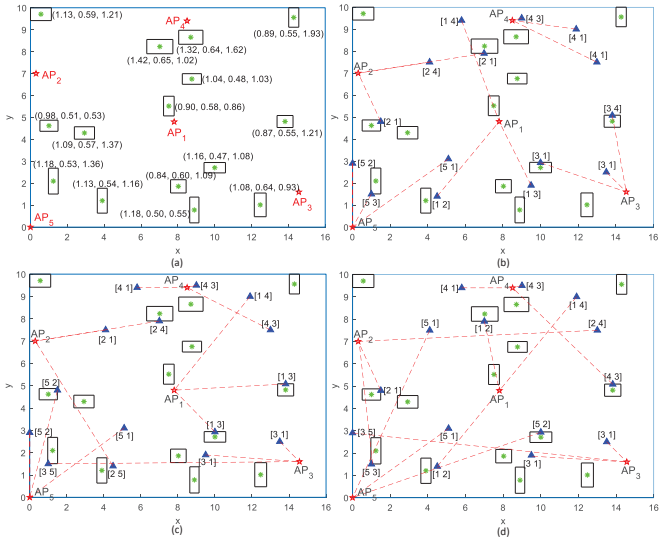

Fig. 6. (a) A mmWave WLAN scenario; (b) mRI results; (c) mRI-MP results; (d) A-mRI results.

4) Other simulation parameters: All evaluations are done at the mmWave frequency of 60 GHz with a 2.16 GHz bandwidth, and the transmission power at AP side is 10 dBm. To build an accurate channel model for indoor mmWave communication, we adopt a widely-used log-distance path loss model extended to include multipath and shadowing components:

$$L(d) = L(d_0) + 10 \cdot n \cdot \log_{10}(\frac{d}{d_0}) + X_\Omega + X_s \quad [\text{dB}]. \quad (21)$$

In Eq. (21), $L(d)$ is the path loss in decibels at separation distance d, $L(d_0)$ represents the path loss at a reference distance d_0, n is the path loss exponent. In the NLoS condition, X_s represents a shadowing term resulting from the penetration

loss of the signal traveling through an obstacle, and X_Ω represents the normal distribution of multipath fading, where Ω is the standard deviation. Note that when the communication link is in LoS condition, we also consider a fading coefficient as the channel gain drawn from a known Rician distribution ($\kappa_{dB} = 5.57$) based on [14], [40], which mimics a more dynamic mmWave channel. Here we collect the average of several sets of experimental estimations of path loss (including the path loss exponent and distribution of multi-path fading), where all experiments are performed with LoS connections in the lab environment [3], and n and Ω are set as 2 and 4.68, respectively. The shadowing term X_s is determined from obstacles' locations, dimensions, and materials, based on [41]. According to IEEE 802.11ad protocol, we assume that each mmWave AP adopts the single carrier PHY, which supports 12 modulation and coding schemes [8].

In what follows, we first randomly generate several network scenarios with different obstacle and client distributions, and then evaluate different network performance metrics with proposed association approaches. By performing the simulation with client mobility in network scenarios, each data point in following figures is the averaged result of 60 simulation runs.

B. Network blockage tolerance

In this part, we evaluate whether or not our proposed algorithms can maintain high-rate (i.e., LoS) connections for each client in the presence of both fixed and moving obstacles. During each simulation run, we periodically stop the simulation and evaluate the network conditions. Here, network blockage tolerance rate (BTR) [42] is adopted as the metric for evaluation, which represents the percentage of evaluated moments in which *all* clients have LoS connections out of all evaluated moments.

First, we investigate how the client density affects the network robustness. With the specific client-mobility factor η = 0.3, we evaluate the performance of different AP association schemes, and the results are reported in Fig. 7.

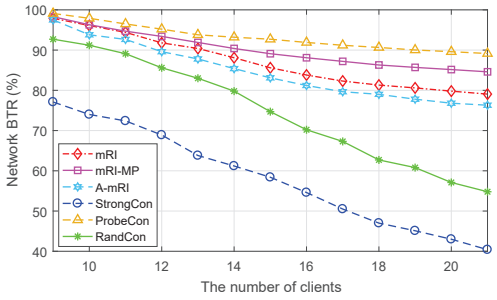

Fig. 7. Network BTR vs. client density.

Fig. 7 shows the performance comparisons between our algorithms and other existing AP association approaches. Among all schemes, we observe that the network BTR decreases as the client density increases, which is because there are more clients with mobility acting as moving obstacles, which increases the overall likelihood of blockage. Compared to *RandCon* and *StrongCon*, our algorithms offer higher blockage tolerance, with a network BTR of around 80% even with a high density of clients, while the network BTRs of *RandCon* and *StrongCon* are only 54% and 40%, respectively, at the same density. The *StrongCon* scheme shows the worst performance since only the RSS is evaluated as the metric to assign AP for each client without considering potential blockage effects. It is observed that *ProbeCon* provides the best blockage tolerance, albeit at the cost of each client dynamically searching all available APs by probing channel conditions on every transmission. However, it is noted that our algorithms can achieve similarly high performance as *ProbeCon* does, where the performance gap is less than 4% for the mRI-MP scheme. Since our algorithms perform a static assignment, they do not incur any probing overhead and, as we show later, they offer better performance than *ProbeCon* in other important dimensions.

We now focus on the performance comparison among our different algorithms in Fig. 7. It is worth noting that the network BTR of the mRI-MP scheme is significantly higher than for the mRI scheme. Thus, having the knowledge of mobility patterns of clients provides notable performance gains, since this allows clients to associate with the best APs to provide LoS connections at places where they are more likely to go. Additionally, there is a little performance decrease (less than 3%) with the A-mRI scheme as compared to the mRI scheme, since the A-mRI scheme is designed to improve load balancing across APs (as shown in Sec. V-D) but does so by trading off some blockage tolerance, i.e., a few clients may not associate to the APs with maximum robustness index.

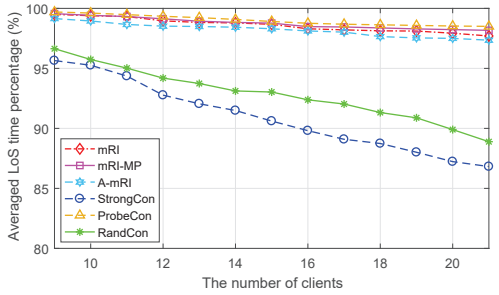

Fig. 8. LTP vs. client density.

We also evaluated the averaged LoS time percentage (LTP) for each client, which is the percentage of evaluated simulation moments at which a given client has a LoS connection out of all evaluated moments. As shown in Fig. 8, we observe that all of our algorithms provide good LTP performance (always over 97% even with high client densities), which is nearly the same as *ProbeCon*. Thus, in these simulations, high-rate connectivity is maintained almost all of the time for each client with our proposed AP association schemes.

Next, we investigate how the client-mobility factor η affects the network robustness. We know that η denotes how frequent the clients will leave home locations and move around, thus the larger η indicates that clients have more potential to move.

By performing different simulation cases with 15 clients, we evaluate the network BTR of different schemes with increasing η. As shown in Fig. 9, the performance of our algorithms is always superior to that of *StrongCon* and *RandCon*, and is also nearly as good as *ProbeCon*, particularly the mRI-MP scheme. In addition, in comparing among our different algorithms, it is observed that the mRI-MP scheme provides better network robustness as compared to the AP association schemes without considering mobility patterns of clients, such as the mRI and A-mRI schemes. This result confirms that taking into account the client-mobility information for AP association can provide substantial benefits for network robustness.

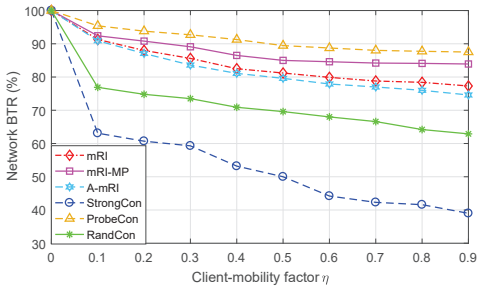

Fig. 9. Network BTR vs. client-mobility factor.

C. Throughput performance

In this part, we investigate the throughput performances of the proposed schemes and the comparison schemes. Recall that in the *StrongCon* scheme, each client associates to the AP with the strongest RSS and maintains that association for all data transmissions and in the *ProbeCon* approach, each client associates to the best AP by probing the channel conditions before every transmission. For *RandCon* and for our schemes, each client is assigned to a primary AP and backup AP according to a random selection strategy (*RandCon*) or using our strategies defined in Section V. For these schemes, clients track both primary and backup APs as they move around the room, and fast switching is performed from the current AP to the other AP whenever a blockage occurs.

To calculate the throughputs of these approaches, a few parameters need to be chosen. For the *ProbeCon* scheme, a fixed overhead of 2% is applied to every transmission, which is in accordance with the results presented in [14]. Based on [26]–[28], the overhead of beam tracking and switching between primary and alternative links is 0.55–0.7%. For our schemes and *RandCon*, when the client is stationary and a LoS connection to the current AP is maintained, there is no overhead added in the simulations. In these two schemes, while clients are moving or if the client is stationary but the LoS connection to the current AP is lost, a conservative overhead of 0.7% is applied to every transmission. Note that, due to the use of narrow-beam directional antennas, the interference effects among different transmission links are ignored. Prior work has shown that the impact of side lobe interference is small. Furthermore, any such impacts should affect all schemes in a similar way so that relative performances among them would be substantially unchanged by adding side lobe effects.

First, with the specific $\eta = 0.3$ and varied client densities, we evaluate the average user throughput that indicates the averaged data bytes received by each user per second.

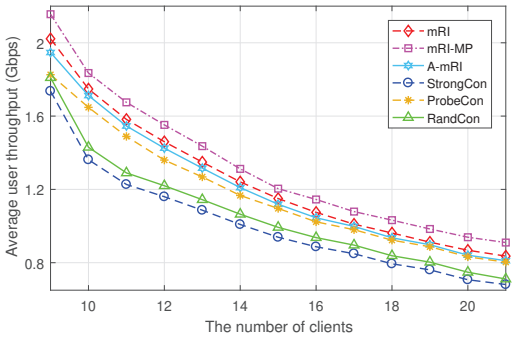

Fig. 10. Throughput vs. client density.

Fig. 10 shows the throughput performance over different multi-AP association schemes. As is expected, the average user throughput decreases when the number of client increases since more clients are going to share the same mmWave AP. It is observed that our schemes maintain higher user throughput performance than the other approaches. In particular, as compared to *ProbeCon*, the average user throughput can be improved by around 12%, 6%, and 3% with our mRI-MP, mRI, and A-mRI schemes, respectively. This is because our approaches eliminate the overhead for dynamically probing the channel condition every time, by statically assigning APs with the maximum LoS probability for each client based on the detailed blockage analysis of the environment.

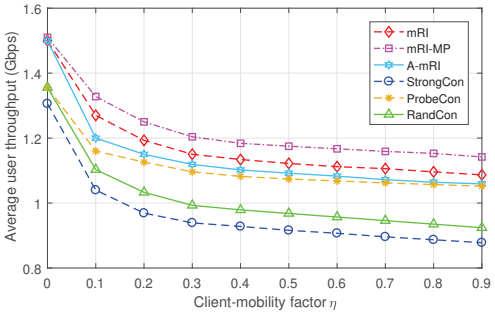

Fig. 11. Throughput vs. client-mobility factor.

Additionally, we evaluate the impact of client-mobility factor η on the throughput performance with N_u = 15 and the results are shown in Fig. 11. We observe that the throughput drops slightly as η increases since more clients tend to move around in the room, which aggravates the blockage effects. However, our proposed schemes can still maintain much higher user throughput and outperform other approaches, especially the mRI-MP scheme which makes use of knowledge of the mobility patterns of clients.

D. Fairness and load balancing

In addition to the blockage tolerance and throughput performance, here we also show some secondary benefits brought by our approach. First, we investigate whether or not it can offer

fair resource allocations for clients in mmWave WLANs. The time-based fairness index is used to evaluate if all clients can be allocated equal channel occupancy time, and the fairness metric is defined as $F = (\sum_{i \in U} T_i)^2 / (N_u \cdot \sum_{i \in U} T_i^2)$, where T_i is the time slot duration allocated to each client, and N_u is the number of clients.

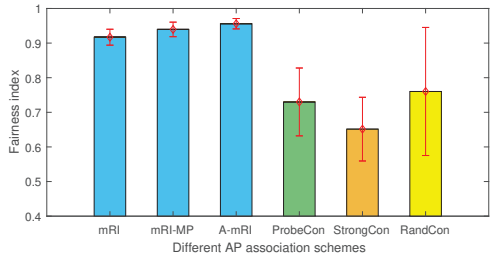

Fig. 12. Fairness comparisons among different schemes.

With N_u = 15 and η = 0.3, Fig. 12 shows that our approaches have significantly better fairness than the other schemes. In particular, the fairness indexes of all of our proposed schemes are above 0.9, while the other schemes are all below 0.75 in fairness.

We also evaluate the load balancing performance with proposed schemes. The maximum load utilization L_{max} (see Sec. IV-A) is used as the metric to qualitatively reflect the congestion of network, where a higher L_{max} causes more network congestion and unbalanced resource usage. Here, the data demand of each client is assumed to follow the normal distribution $\mathcal{N}(D_\mu, D_\sigma)$. As the results show in Fig. 13, all of our schemes provide better load balancing across APs than other approaches, because we included consideration of the load in the proposed HRS and AHRS algorithms. With the growth of expected traffic demand of each client, the performance benefits provided by our proposed schemes become more obvious, while other schemes are likely to cause more severe network congestion, because clients have a higher likelihood of selecting the same AP for their connections.

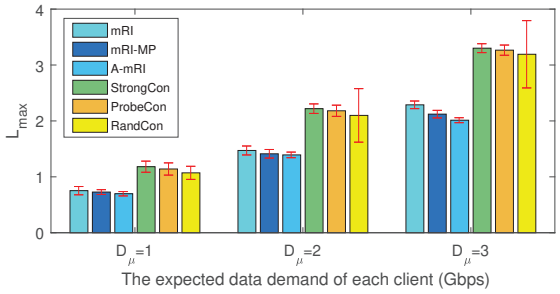

Fig. 13. $\mathrm{L_{max}}$ vs. expected data demand of each client ($D_\sigma = 0.3$).

To better illustrate the load balancing benefits of the A-mRI scheme, we vary η and evaluate the performance of mRI and A-mRI, which both operate under the assumption of no knowledge of client mobility patterns. With D_μ = 2, D_σ = 0.3, and two different client densities, the results are reported in Fig. 14. First, it is observed that mRI scheme does not perform well when η becomes large. This is because, as η increases, the client-mobility tolerance P_{CMT} becomes a more dominant factor in the derived robustness index, and without any mobility pattern information, most of clients are likely to be assigned with the same APs having the similar P_{CMT}, which causes an uneven AP-load distribution. However, as is expected, the A-mRI scheme always offers good load balancing across APs, because it incorporates the load as a primary factor in determining the association. The performance benefits of A-mRI become larger as both η and client density increase. Thus, if load balancing is a primary concern in some dynamic and large-scale network scenarios, it is advisable to adopt the A-mRI scheme for AP association. However, as a trade-off, the blockage tolerance and throughput performance might decrease slightly, as was shown in Fig. 7 and Fig. 10.

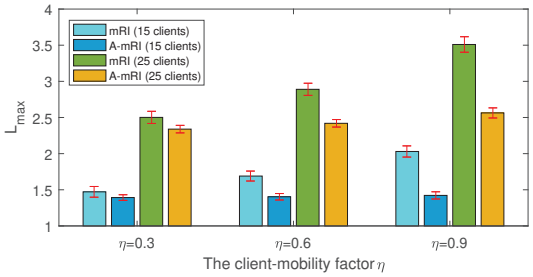

Fig. 14. $\mathrm{L_{max}}$ vs. client-mobility factor η with 15 and 25 clients.

E. Performance of AHRS approach

In the AHRS approach (see Sec. IV.B), both the optimal method ($\mathrm{AHRS_{opt}}$) and the heuristic A-mRI can be used to obtain results. Here we compare the performance of the heuristic scheme against the optimal solution. With different obstacle distributions, we generate network scenarios with different number of APs and clients (with η = 0.3). As shown in Fig. 15, it is observed that A-mRI provides near-optimal results, with performance gaps of less than 2% even for larger networks.

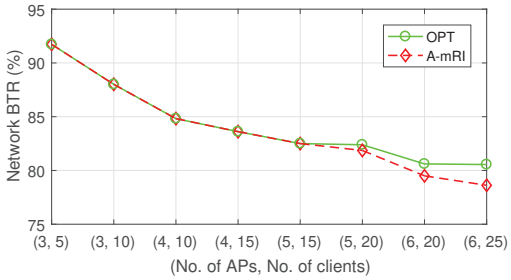

Fig. 15. Comparisons between optimal method and Alg. 2 vs. network scale.

However, when comparing the running time to compute an AP association for the two methods[5], we found that the execution time increases rapidly with network size. The running time ranges from 4.74 minutes to 37.52 minutes over the data

[5]We evaluate the running time on an Intel(R) Core(TM) i5-6200U 2.3GHz CPU workstation with 2 cores and 4 logical processors.

points shown in Figure 15, which makes it impractical for timely configuration in real network scenarios. By comparison, A-mRI only takes 3.87 seconds to 16.96 seconds over the same data points. Thus, A-mRI has execution times that are practical while experiencing almost no drop-off in blockage tolerance, as compared to the optimal scheme.

F. Discussion

Here we summarize the key findings from this section:

- When comparing a basic static method (mRI) against the dynamic channel-probing approach, we see that the static approach can achieve higher throughput (due to lower run-time overhead) with only a small reduction in blockage tolerance.
- If client mobility patterns are known, this information can be used to boost the performance of the static approach further, resulting in a more than 10% increase in throughput compared to dynamic probing while achieving almost the same blockage tolerance.
- All our proposed approaches achieve significantly better fairness and load balancing than existing approaches for typical cases.
- For scenarios with high mobility and a load balancing requirement, our A-mRI scheme is a better choice since it always maintains very good load balancing across APs at the cost of a modest reduction in blockage tolerance.

VII. Conclusion

In this paper, we studied the multi-AP association problem in mmWave WLANs. Based on a detailed analysis of blockage tolerance under mobility conditions, several novel association schemes were proposed to maximize connection reliability for all clients in a WLAN. Numerical simulation results showed that our AP association policies can substantially improve network robustness, user throughput, load balancing, and fairness, as compared to other AP association methods.

Acknowledgement

This research was supported in part by the National Science Foundation through Award CNS–1813242.

References

[1] X. Wang, et al. “Millimeter wave communication: A comprehensive survey", *IEEE Communications Surveys & Tutorials* 20.3, 2018.
[2] S. Sur, I. Pefkianakis, X. Zhang, et al. “Wifi-assisted 60 GHz wireless networks", *ACM Int’l Conf. Mobile Computing and Networking*, 2017.
[3] P. Smulders. “Statistical characterization of 60-GHz indoor radio channels", *IEEE Transactions on Antennas and Propagation*, 2009.
[4] Y. Liu and D. Blough,“Analysis of blockage effects on roadside relay-assisted mmWave backhaul networks," *IEEE ICC*, 2019.
[5] G. Hosseinabadi, and V. Nitin. "Concurrent-MAC: Increasing concurrent transmissions in multi-AP wireless LANs", *ACM International Conference on Mobile Computing & Networking*, 2013.
[6] Z. Yang, et al. “Sense and deploy: Blockage-aware deployment of reliable 60 GHz mmwave wlans", *IEEE International Conference on Mobile Ad Hoc and Sensor Systems*, 2018.
[7] Y. Liu, Y. Jian, R. Sivakumar, and D. Blough. “Optimal access point placement for multi-AP mmWave WLANs," *ACM Modeling, Analysis and Simulation of Wireless and Mobile Systems*, 2019.
[8] IEEE Std 802.11ad-2012, 2012. URL:https://ieeexplore.ieee.org/stamp/stamp.jsp?arnumber=6392842.
[9] X. Qin, et al. “On AP Assignment and Transmission Scheduling for Multi-AP 60 GHz WLAN", *IEEE International Conference on Mobile Ad Hoc and Sensor Systems*, 2017.
[10] X. Zhang, et al. “Improving network throughput in 60GHz WLANs via multi-AP diversity", *IEEE Int’l Conference on Communications*, 2012.
[11] B. Soleimani and M. Sabbaghian,“Cluster-based resource allocation and user association in mmwave femtocell networks", *IEEE Transactions on Communication*, 2018.
[12] F. Zhou, et al. “Making the right connections: Multi-AP association and flow control in 60GHz band", *IEEE INFOCOM*, 2018.
[13] G. Athanasiou, et al. “Optimizing client association for load balancing and fairness in millimeter-wave wireless networks", *IEEE/ACM Transactions on Networking* 23.3 (2014): 836-850.
[14] D. Ramirez, et al. “On opportunistic mmWave networks with blockage", *IEEE Journal on Selected Areas in Communications* 2017: 2137-2147.
[15] N. Chang and M. Liu, “Optimal channel probing and transmission scheduling for opportunistic spectrum access", *Trans. on Netw.*, 2009.
[16] H. Jiang, L. Lai, R. Fan, and H. V. Poor, “Optimal selection of channel sensing order in cognitive radio", *IEEE Trans. Wireless Commun.*, 2009.
[17] A. Gudipati, et al. “SoftRAN: Software defined radio access network", *ACM SIGCOMM Workshop*, 2013.
[18] X. Qin, et al. “Joint user-AP association and resource allocation in multi-AP 60 GHz WLAN", *IEEE Trans. on Vehicular Technology*, 2019.
[19] S. Sur, et al, “60 GHz indoor networking through flexible beams: A link-level profiling", *ACM SIGMETRICS*, 2015.
[20] E. Kocan, L. Aleksandra, et al. “Macro diversity for mmWave cellular communications in indoor environment", *Computer Networks*, 2019.
[21] M. Giordani, M. Mezzavilla, S. Rangan, and M. Zorzi. “An efficient uplink multi-connectivity scheme for 5G millimeter-wave control plane applications", *IEEE Transactions on Wireless Communications*, 2018.
[22] M. Gapeyenko, et al. “On the degree of multi-connectivity in 5G millimeter-wave cellular urban deployments", *IEEE Transactions on Vehicular Technology*, 2018.
[23] M. Giordani, et al. “Multi-connectivity in 5G mmWave cellular networks", *IEEE Mediterranean Ad Hoc Networking Workshop*, 2016.
[24] M. Gerasimenko, et al. “Capacity of multiconnectivity mmWave systems with dynamic blockage and directional antennas", *IEEE Transactions on Vehicular Technology*, 2019.
[25] S. Kang, et al. “A dual-connection based handover scheme for ultra-dense millimeter-wave cellular networks", *IEEE Global Comm.*, 2019.
[26] M. Rasekh, et al. “Noncoherent mmWave path tracking", *ACM International Workshop on Mobile Computing Systems and Applications*. 2017.
[27] B. Gao et al., “Double-link beam tracking against human blockage and device mobility for 60-GHz WLAN", *IEEE WCNC*, 2014.
[28] J. Palacios, D. Donno, et al. “Tracking mm-Wave channel dynamics: Fast beam training strategies under mobility", *IEEE INFOCOM*, 2017.
[29] O. Karimi, J. Liu, and J. Rexford. “Optimal collaborative access point association in wireless networks", *IEEE INFOCOM*, 2014.
[30] R. Cowan. “Objects arranged randomly in space: An accessible theory", *Adv. Appl. Probability* [Online].
[31] T. Bai, R. Heath, “Coverage and rate analysis for millimeter-wave cellular networks”, *IEEE Trans. on Wireless Communications*, 2015.
[32] C. Song, et al. “Modeling the scaling properties of human mobility", *Nature Physics* 6.10 (2010): 818.
[33] Y. Liu and D. Blough. “Technical report for grid-based shadowing search method", (available to reviewers at: http://blough.ece.gatech.edu/TR-Multi-AP-indoor.pdf).
[34] Y. Lee, K. Kim, and Y. Choi. “Optimization of AP placement and channel assignment in wireless LANs", *IEEE LCN*, 2002.
[35] “IBM ILOG CPLEX", https://www.ibm.com/products/ilog-cplex-optimization-studio.
[36] “Bonmin", https://projects.coin-or.org/Bonmin.
[37] V. Norkin, et al. “A branch and bound method for stochastic global optimization", *Mathematical programming* 83.1-3 (1998): 425-450.
[38] P. Santi, “Mobility models for next generation wireless networks: Ad Hoc, vehicular and mesh networks", *John Wiley & Sons*, 2012.
[39] M. Kim, D. Kotz, and S. Kim. “Extracting a mobility model from real user traces", *Dartmouth Digital Commons*, 2006.
[40] J. Reig, et al. “Fading evaluation in the 60 GHz band in line-of-sight conditions", *International Journal of Antennas and Propagation*, 2014.
[41] J. Lu, et al. “Propagation characterization of an office building in the 60 GHz band", *IEEE Antennas and Propagation*, 2014.
[42] Y. Liu, Q. Hu, and D. Blough, “Blockage avoidance in relay paths for roadside mmWave backhaul networks", *IEEE PIMRC*, 2018.